A Tale of Two Populations: The Contribution of Merger and Secular Processes to the Evolution of Active Galactic Nuclei

A. R. Draper and D. R. Ballantyne

Center for Relativistic Astrophysics, School of Physics, Georgia Institute of Technology, Atlanta, GA 30332

aden.draper@physics.gatech.edu

ABSTRACT

Due to the co-evolution of supermassive black holes and their host galaxies, understanding the mechanisms that trigger active galactic nuclei (AGN) are imperative to understanding galaxy evolution and the formation of massive galaxies. It is observationally difficult to determine the trigger of a given AGN due to the difference between the AGN lifetime and triggering timescales. Here, we utilize AGN population synthesis modeling to determine the importance of different AGN triggering mechanisms. An AGN population model is computed by combining an observationally motivated AGN triggering rate and a theoretical AGN light curve. The free parameters of the AGN light curve are constrained by minimizing a χ^2 test with respect to the observed AGN hard X-ray luminosity function. The observed black hole space density, AGN number counts, and X-ray background spectrum are also considered as observational constraints. It is found that major mergers are not able to account for the entire AGN population. Therefore, non-merger processes, such as secular mechanisms, must also trigger AGN. Indeed, non-merger processes are the dominant AGN triggering mechanism at $z \lesssim$ 1–1.5. Furthermore, the shape and evolution of the black hole mass function of AGN triggered by major mergers is intrinsically different from the shape and evolution of the black hole mass function of AGN triggered by secular processes.

Subject headings: galaxies: active — galaxies: Seyfert — galaxies: quasars: general — X-rays: diffuse background

1. Introduction

In less than a decade it was determined that not only do all massive galaxies harbor a supermassive black hole at their center (Kormendy & Richstone 1995), but also that

the evolution of the galaxy is intrinsically linked to the growth of the central black hole (e.g., Magorrian et al. 1998; Tremaine et al. 2002). However, the mechanism responsible for the co-evolution of a supermassive black hole and its host galaxy is still under investigation. As accreting supermassive black holes, generally referred to as active galactic nuclei (AGN), can, over their lifetime, radiate an amount of energy comparable to the binding energy of their host galaxy (e.g., Silk & Rees 1998; Fabian 1999; Alexander et al. 2010), it is believed that this AGN feedback will affect star formation in the host galaxy (e.g., Fabian 1999; Hopkins et al. 2006a; Lagos et al. 2008; Trichas et al. 2009; Bertone et al. 2010; Hambrick et al. 2011; Hocuk & Spaans 2011). Galaxy wide processes can also affect the central supermassive black hole. For example, theoretical and observational evidence suggests that AGN can be triggered by major mergers of massive gas rich galaxies (e.g., Sanders et al. 1988; Hernquist et al. 1989; Carlberg 1990; Kauffmann & Haehnelt 2000; Hopkins et al. 2006a) or by secular processes not connected to major mergers, such as supernova winds, stellar bars, cold-flow accretion, interactions with other massive galaxies or satellite galaxies, or minor mergers (e.g., Crenshaw et al. 2003; Kormendy & Kennicutt 2004; Vittorini et al. 2005; Davies et al. 2007; Pierce et al. 2007; Chen et al. 2009; Kumar & Johnson 2010; Bournaud et al. 2011; Orban de Xivry et al. 2011).

Simulations show that mergers of gas rich galaxies cause gas and dust to lose angular momentum and fall into the central regions of the galaxy (e.g., Barnes & Hernquist 1996). The resulting nuclear gas reservoir will be consumed by star formation in the host bulge and accretion flows onto the resident supermassive black hole (Hopkins et al. 2006a,b). According to the galaxy evolution model explored by Hickox et al. (2009), AGN feedback will then evolve the AGN host galaxy across the color-magnitude diagram (CMD) from the massive end of the blue cloud, through the green valley, and onto the red sequence (but see Schawinski et al. 2009 and Cardamone et al. 2010). Secular processes, such as supernova explosions, stellar bars, minor mergers and interactions, will also release angular momentum from gas and dust leading to a similar reservoir of gas in the central region of the galaxy (e.g., Crenshaw et al. 2003; Davies et al. 2007; Chen et al. 2009; Orban de Xivry et al. 2011). Despite mergers and secular mechanisms both leading to the accumulation of gas and dust deep in the galactic potential well, mergers and secular processes have very different galaxy wide effects and roles in galaxy evolution. Major mergers are violent processes which, as with the Antennae galaxies, can destroy galactic structure, causing the merger remnant to relax into a bulge-dominated system (e.g., Hopkins & Hernquist 2006). Secular evolution, however, is not likely to disturb the morphology or large-scale structure of the host galaxy (see Georgakakis et al. 2009). Despite the systemic differences between galaxy evolution and AGN activity due to major mergers and secular processes, it is difficult to observationally determine which mechanism is responsible for a given AGN; tidal tails are often faint, bulge-

dominated systems can be re-triggered by secular processes, and the timescales for AGN activity tend to be longer than the timescales for a merger remnant galaxy to dynamically relax (Schawinski et al. 2010a).

Despite the observational difficulties in determining how a particular AGN has been triggered, there is observational evidence that major mergers are not the dominant AGN triggering mechanism, at least not at $z \lesssim 2$. By determining the Sérsic indices of massive galaxies at $z = 2$–3, Weinzirl et al. (2011) found that $\sim 65\%$ of AGN hosts at this redshift range have Sérsic indices indicative of disky morphologies. Observations also show that in the redshift ranges $z = 1.5$–3 (Schawinski et al. 2011) and $z = 1.5$–2.5 (Kocevski et al. 2012), the majority of moderate luminosity AGN are hosted by disk galaxies. By considering galaxy pairs at $z \lesssim 2$, Williams et al. (2011) find that the wet major merger rate is too low to account for the majority of AGN activity at $z \lesssim 2$. When investigating AGN in zCOSMOS, Silverman et al. (2011) found that $\sim 20\%$ of moderate luminosity AGN at $0.25 < z < 1.05$ are in close pairs, and thus were likely triggered by galaxy interactions. Cisternas et al. (2011) argue that AGN are as likely as quiescent galaxies to show signs of a recent merger at $z < 1$, and thus mergers cannot be connected to AGN activity at this redshift range. Georgakakis et al. (2009) investigate the morphology of AGN hosts and find that AGN hosted by disk galaxies contribute $\sim 25\%$ of the AGN luminosity density at $z \approx 0.8$. They conclude, therefore, that a large fraction of $z \sim 1$ AGN are triggered by mechanisms unrelated to major mergers. Cardamone et al. (2010) found that when AGN host galaxy colors are corrected for dust extinction, there is a bi-modality of AGN host galaxy colors at $z \sim 1$, suggesting that there are two modes of AGN activity at this redshift range. When modeling the AGN population by considering mergers of massive dark matter halos, Shen (2009) find that secular AGN activity is necessary at $z < 0.5$ to account for the observed AGN population. Koss et al. (2010) recently found that $\sim 20\%$ of *Swift*/BAT AGN at $z < 0.05$ are hosted by galaxies with disturbed morphologies indicative of a recent major merger and an additional 6% of *Swift*/BAT AGN are in close pairs suggesting these AGN were triggered by galaxy interactions. Thus, it appears that both major mergers and secular processes must contribute to the AGN activity observed at $z \lesssim 2$. If secular triggers dominate the AGN population at $z \lesssim 2$, current understanding of the stochastic fueling of secular mechanisms is insufficient to explain the high luminosity of quasars observed at $z \lesssim 2$ (Hopkins & Hernquist 2006). However, Bournaud et al. (2011) recently showed that, at least at high redshift, it is possible for cold-flow accretion to trigger moderate luminosity AGN with occasional bright episodes. Thus, phenomenological models of the AGN population may provide an important tool for understanding the importance of merger and secularly triggered AGN at various redshift and luminosity ranges.

Here, a model of the AGN population is calculated using an empirically motivated space

density of AGN triggered at each redshift and a theoretical AGN light curve. We consider whether major mergers or secular mechanisms alone can account for the observed AGN hard X-ray luminosity function (HXLF), AGN number counts, black hole space density, and the X-ray background (XRB) spectrum. In Section 2 the details of the AGN model, including the triggering rate, light curve, and black hole mass functions utilized, are described. Section 3 explains the calculations completed to compare the model against observations. We then consider the model results if AGN are a single population (Section 4) or two populations (Section 5). The results are discussed and summarized in Sections 6 and 7. A ΛCDM cosmology is assumed with $H_0 = 70$ km s^{-1} Mpc^{-1} and $\Omega_\Lambda = 1.0$ - $\Omega_M = 0.7$.

2. The AGN Population Model

In order to model the evolution of the AGN HXLF, three ingredients are necessary. To determine the space density of triggered AGN, an empirically based major merger rate is used. Once triggered, the AGN Eddington ratio, $\lambda = L_{bol}/L_{Edd}$, where L_{bol} is the bolometric luminosity and L_{Edd} is the Eddington luminosity, is evolved using a theoretically motivated light curve. The active black hole mass function (ABHMF) and the Marconi et al. (2004) bolometric correction are then used to convert from Eddington ratio to 2–10 keV luminosity, L_X. These three ingredients are described in detail below.

2.1. Triggering Rate

In order to determine the space density of AGN triggered at each redshift, the space density of gas rich massive galaxies at redshift z must be calculated. First, the minimum stellar mass of a massive galaxy, M_*^{min}, at z is derived by parametrizing the median mass of ultra-luminous infrared galaxies (ULIRGS) as a function of redshift (Treister et al. 2010a), which gives

$$M_*^{min}(z) = 5 \times 10^{11}(1.0 + z)^{-1.5} M_\odot. \tag{1}$$

The space density of massive galaxies at z, $N_{gal}(M_* > M_*^{min}(z))$, in Mpc^{-3}, can then be calculated by integrating the stellar mass function from $M_*^{min}(z)$ to $M_*^{max} = 10^{12.5}$ M$_\odot$, such that

$$N_{gal}(M_* > M_*^{min}(z)) = \int_{M_*^{min}(z)}^{M_*^{max}} \frac{d\Phi_{gal}(M_*, z)}{d \log M_*} d \log M_*, \tag{2}$$

where $d\Phi_{gal}/d \log M_*$ is the stellar mass function (SMF) of Pérez-González et al. (2008) for $z \lesssim 4$. The dependence of the results on the SMF is considered in Sections 4.1 and 4.2. To determine the space density of gas rich massive galaxies, the fraction of gas rich galaxies at

z, $f_g(z)$, must be determined. Considering observations of the GOODS fields (Dahlen et al. 2007), Treister et al. (2010a) find that $f_g(z)$ can be parametrized as

$$f_g(z) = \begin{cases} 0.11(1+z)^{2.0} & z \leq 2 \\ 1 & z > 2 \end{cases}. \tag{3}$$

Thus the space density, in Mpc^{-3}, of potential AGN host galaxies at redshift z is $f_g(z)N_{gal}(M_* > M_*^{min}(z))$.

The space density of AGN triggered by a merger at redshift z is then calculated by multiplying the space density of potential AGN host galaxies at z by the fraction of massive galaxies which will undergo a merger at z. Following Hopkins et al. (2010a), who derive the major merger rate per galaxy per Gyr, $d^2\Psi/dt\,dN$, from simulations and observational constraints, we parametrize $d^2\Psi/dt\,dN$ as

$$\frac{d^2\Psi}{dt\,dN} = A(M_*^{min})(1.0+z)^{\beta(M_*^{min})}, \tag{4}$$

where

$$A(M_*) = 0.02\left[1 + \left(\frac{M_*}{2 \times 10^{10} M_\odot}\right)^{1/2}\right]\mathrm{Gyr}^{-1} \tag{5}$$

and

$$\beta(M_*) = 1.65 - 0.15\log\left(\frac{M_*}{2 \times 10^{10} M_\odot}\right). \tag{6}$$

Here the major merger is said to occur upon the coalescence of the two similarly massive galaxies (Hopkins et al. 2010b). By assuming that every major merger leads to an AGN event, with a negligible time delay between the merger and the triggering of the AGN activity, the space density of AGN triggered by major mergers, dN_{merg}, at redshift z is

$$dN_{merg}(z) = \frac{d^2\Psi}{dN\,dt}N_{gal}(M_* > M_*^{min}(z))\,f_g(z)\,dt\,\mathrm{Mpc}^{-3}. \tag{7}$$

The rate at which AGN are triggered through secular processes, such as galaxy interactions, cold gas accretion, and internal disk instabilities, is calculated in a similar manner. For AGN triggered by secular processes, $M_*^{min}(z) = 5 \times 10^9$ $\mathrm{M}_\odot$, in agreement with the findings of Schawinski et al. (2010b). The fractional rate of massive gas rich galaxies which are triggered through secular processes every Gyr, f_{sec}, is assumed to be constant with redshift. Yamada et al. (2009) found that the fraction of galaxies with $M_* > 10^{11}$ $\mathrm{M}_\odot$ hosting AGN, which are triggered through both secular processes and mergers, is $\sim$0.3. As the fraction of AGN triggered by secular processes is poorly constrained observationally, and we are considering galaxies with $M_* > 5 \times 10^9$ $\mathrm{M}_\odot$, the constraint $f_{sec} \ll 0.3$ Gyr^{-1} is used. The

specific value of f_{sec} is set by calculating the predicted AGN HXLF and minimizing a χ^2 test which compares against the observed HXLF. The space density of AGN triggered by secular mechanisms, dN_{sec}, at redshift z is then

$$dN_{sec}(z) = f_{sec} \, N_{gal}(M_* > M_*^{min}(z)) \, f_g(z) \, dt \, \mathrm{Mpc}^{-3}. \tag{8}$$

2.2. AGN Light Curve

Once the AGN has been triggered, its Eddington ratio is used to parametrize the accretion as a function of time since the AGN was triggered. While there is evidence that AGN are an intermittent phenomenon, Treister et al. (2010a) show that quasars can grow most of their black hole mass in a single, merger triggered event. Therefore, a single-peaked light curve is assumed.

Based on hydrodynamical simulations, Hopkins & Hernquist (2009) suggest

$$\lambda(t) = \left[1 + (|t|/t_Q)^{1/2}\right]^{-2/\beta}, \tag{9}$$

where $t = t_{on} - t_Q$, where t_{on} is the time since the AGN was triggered, $t_Q = t_0 \eta^{\beta}/(2\beta \ln 10)$, and t_0, η, and β are fitting parameters which describe the quasar lifetime, maximum Eddington ratio, and light curve slope, respectively[1].

2.3. Active Black Hole Mass Function and Its Evolution

By combining the triggering rate and light curve, the space density of AGN with Eddington ratio λ can be calculated at any redshift $z \lesssim 4$. However, to compute model predictions that can be compared to observational constraints, the black hole mass must be used to convert Eddington ratios into bolometric luminosities. Once the bolometric luminosity is computed, the Marconi et al. (2004) bolometric correction is used to determine L_X. The distribution of black hole masses is determined by the fractional active black hole mass function (ABHMF) at z, which describes the fraction of active black holes at redshift z with black hole mass $M_\bullet$.

---

[1]For completeness, a wide variety of light curves were tested, including a constant λ, a monotonic linearly increasing or decreasing λ, a monotonic exponentially increasing or decreasing λ, a linearly increasing followed by a linearly decreasing λ, and an exponentially increasing followed by an exponentially decreasing λ. However, these light curve models were unable to match the shape of the AGN HXLF.

Two ABHMFs are considered. The first ABHMF is a Gaussian fit to the combined type 1 and type 2 AGN ABHMF at $z \sim 0.15$ observed by Netzer (2009). The second ABHMF considered is a Schechter function with the same slope and critical mass, M_{crit}, as the black hole mass function described by Merloni & Heinz (2008). Both ABHMFs are considered over the range $\log(M_\bullet^{min}/M_\odot) = 5.95$ and $\log(M_\bullet^{max}/M_\odot) = 10.55$. A black hole with $M_\bullet < M_\bullet^{min}$ would need to accrete at Eddington ratio $\lambda \gtrsim 0.1$ to achieve $\log L_X \gtrsim 41.5$. According to the light curve used here, the vast majority of the AGN lifetime is spent at $\lambda < 0.1$. Therefore, black holes with $M_\bullet < M_\bullet^{min}$ are expected to only make a very small contribution to the observed AGN population (Marconi et al. 2004; Merloni & Heinz 2008). Black holes with $M_\bullet > M_\bullet^{max}$, correspond to $\ll 0.1\%$ of all active black holes according to both the Merloni & Heinz (2008) and Netzer (2009) ABHMFs, in agreement with the maximum black hole mass derived by Natarajan & Treister (2009).

Both the Merloni & Heinz (2008) and Netzer (2009) ABHMFs are derived using scaling relationships to determine black hole masses. These scaling relationships have an intrinsic scatter of $\sim$0.3 dex (Peterson & Bentz 2006; Merloni & Heinz 2008; Netzer 2009). This leads to an uncertainty in the calculated L_X of a factor $\sim 2 \times \lambda$. For the majority of sources, $\lambda < 0.1$, thus the uncertainty introduced by the ABHMF is a smaller part of the error budget than the uncertainty in the major merger rate, which is a factor $\sim$2.

For both ABHMFs two redshift evolutions are investigated. The first ABHMF evolution uses the continuity equation (Small & Blandford 1992; Merloni & Heinz 2008)

$$\frac{\partial n_M(M_\bullet, t)}{\partial t} + \frac{\partial[n_M(M_\bullet, t)\langle\dot{M}(M_\bullet, t)\rangle]}{\partial M} = 0, \tag{10}$$

where n_M is the ABHMF and $\langle\dot{M}(M_\bullet, t)\rangle$ is the average accretion rate of black holes with mass $M_\bullet$ at time t. By integrating this conservation equation forward and backward in time, using the observed ABHMF as the boundary condition, the ABHMF can be evolved to any redshift z. This evolution assumes that black hole growth occurs through accretion and that binary mergers are not the primary mechanism of black hole growth (e.g., Volonteri et al. 2003). The second ABHMF evolution considered is based on the observations of Labita et al. (2009) who found that the maximum black hole mass of the quasar population increases with redshift. Thus, $M_\bullet^{crit}(z) = M_\bullet^{crit}(0)(1.0 + z)^{1.64}$. In order to compare the two considered evolutions, a power law is fit to $M_\bullet^{crit}(z)$ of the Merloni & Heinz (2008) ABHMF evolved with the continuity equation and it is found that $M_\bullet^{crit}(z) \approx M_\bullet^{crit}(0)(1.0 + z)^{0.5}$. For both ABHMFs, the ABHMF is re-normalized at each redshift so that integrating over all black hole masses gives 1.

With the observationally determined AGN triggering rate, theoretical Eddington ratio

evolution, and the ABHMF in place, the AGN population at $z < 4$ can be fully modeled[2]. To determine the light curve fitting parameters, t_0, β, and η, the AGN population model must be compared to observational constraints.

3. Calculations and Observational Constraints

In order to constrain the light curve parameters, the AGN population model is compared against the HXLF at five different redshifts, the black hole mass density as a function of redshift, the *Swift/BAT* 15–55 keV AGN counts, the 2–10 keV AGN counts, and the XRB spectrum. The methods used to calculate these quantities are described below.

3.1. AGN HXLF

The HXLF, $d\Phi_X(L_X, z)/d\log L_X$, is computed at five different redshifts, $z = 2.3$, 1.2, 0.6, 0.3, and 0.1. The HXLFs observed by Ueda et al. (2003), La Franca et al. (2005), Silverman et al. (2008), Aird et al. (2010), and Ueda et al. (2011) are each presented in different redshift bins. Therefore, we compute the predicted HXLF at the central redshift of each of the Ueda et al. (2003) redshift bins.

The bolometric AGN luminosity function at redshift z, $d\Phi(L_{bol}, z)/d\log L$, is computed by integrating over the space density of AGN triggered at redshift z_t and, at redshift z, have black hole mass $M_\bullet$ and Eddington ratio λ such that the bolometric luminosity is L_{bol}. Thus,

$$\frac{d\Phi(L_{bol}, z)}{d\log L} = \int_{M_\bullet^{min}}^{M_\bullet^{max}} n_M(M_\bullet, z) d\log M_\bullet \int_z^4 \Phi_\lambda(M_\bullet, z) dz_t, \tag{11}$$

where $\log(M_\bullet^{min}/M_\odot) = 5.95$, $\log(M_\bullet^{max}/M_\odot) = 10.55$, z_t is the triggering redshift, and

$$\Phi_\lambda(M_\bullet, z) = \begin{cases} \frac{dN(z_t)}{d\log L} & \lambda(z, z_t)L_{Edd}(M_\bullet) = L_{bol} \\ 0 & \text{otherwise} \end{cases}, \tag{12}$$

where dN is either dN_{merg} or dN_{sec}. The Marconi et al. (2004) luminosity dependent bolometric correction is then used to convert L_{bol} to L_X.

As the observed HXLF only includes Compton thin AGN, the Compton thick AGN are removed from the calculated HXLF by assuming that one-third of all obscured AGN

---

[2]AGN triggered at $z > 4$ make only a minor contribution to the $z \lesssim 2$ AGN population. Therefore, if the AGN triggered at $z > 4$ are included, the results of this study do not change.

are Compton thick in agreement with the fraction of Compton thick AGN necessary for the Ueda et al. (2003) observed HXLF to be in agreement with the peak of the XRB at ~ 30 keV (Draper & Ballantyne 2009, 2010; Ballantyne et al. 2011). The fraction of Compton thin obscured sources, f_2, is assumed to be a function of luminosity and redshift such that $f_2 \propto (1+z)^a (\log L_X)^{-b}$, where $a = 0.4$ (Ballantyne et al. 2006; Treister & Urry 2006) and $b = 4.7$. The normalization factor is determined by assuming the type 2 to type 1 AGN ratio is 4:1 at $z = 0$ and $\log L_X = 41.5$. Thus, the space density of Compton thick AGN also depends on L_X and, in Mpc^{-3} dex^{-1}, is $(f_2/2)\, d\Phi_X/d\log L_X$.

According to both the Marconi et al. (2004) and Vasudevan et al. (2009) bolometric corrections, to achieve $L_X = 10^{46.5}$ erg s^{-1} it is necessary to have a black hole with mass $\approx 10^{10.7} - 10^{10.9}$ $M_\odot$ accreting at its Eddington rate. Both the Gaussian fit to the Netzer (2009) and the Merloni & Heinz (2008) ABHMF, predict the fraction of active black holes with mass $\sim 10^{11}$ $M_\odot$ is ~ 0, in agreement with the black hole mass upper limit derived by Natarajan & Treister (2009). This strongly suggests that AGN with $L_X \gtrsim 10^{46}$ erg s^{-1} are accreting at super-Eddington rates. The light curve model used allows for $0 \lesssim \lambda \lesssim 1$. Therefore, super-Eddington accretion cannot be taken into account. Thus, the models presented here will necessarily under-predict the $L_X > 10^{46}$ erg s^{-1} observed HXLF data points. For completeness, the HXLF data points at $L_X > 10^{46}$ erg s^{-1} are still taken into account when performing the χ^2 fitting[3].

3.2. Black Hole Mass Density

To calculate the black hole mass density, the Sołtan (1982) argument is used. Thus, the black hole mass density at redshift z, $\rho_\bullet(z)$, is calculated as

$$\rho_\bullet(z) = \int_z^\infty \frac{dt}{dz} dz \int_0^\infty \frac{1-\epsilon}{\epsilon c^2} L_{bol} \frac{d\Phi(L,z)}{d\log L} d\log L \tag{13}$$

where $\epsilon = 0.1$ is the radiative efficiency, c is the speed of light, and $d\Phi(L,z)/d\log L$ is the AGN luminosity function (Yu & Tremaine 2002; Marconi et al. 2004; Treister et al. 2011)[4]. The contribution of Compton thick AGN to the black hole mass density is included. The

---

[3]Exclusion of the three data points at $L_X > 10^{46}$ erg s^{-1} changes the reduced χ^2 values by $\lesssim 0.1$ and does not affect the determination of the light curve parameters.

[4]It is expected that at Eddington ratios $\lambda \lesssim 10^{-2}$, AGN accretion flows become radiatively inefficient and the radiative efficiency decreases with λ (e.g., Cao & Xu 2007). If Equation 1 of Merloni & Heinz (2008) is used to characterize ϵ, the calculated local black hole mass density changes by $< 5\%$ since the majority of black hole growth occurs during radiatively efficient accretion.

predicted black hole mass density is compared to the local black hole mass density observed by Shankar et al. (2009) and the $z \sim 2$ black hole mass density observed by Treister et al. (2010b).

3.3. X-ray Background Spectrum

The XRB spectrum model closely follows that described by Draper & Ballantyne (2009). Instead of inputting the observed luminosity function, the HXLF calculated as described in Section 3.1 is used. Also, a torus reflection component (Gilli et al. 2007) is included which is computed using "reflion" (Ross & Fabian 2005). The Type 2 fraction, f_2, is determined as in Section 3.1. The Compton thick fraction, f_{CT}, is defined as the ratio of the number of Compton thick AGN to the number of Compton thin type 2 AGN, and is set to $f_{CT} = 0.5$, in agreement with the f_{CT} necessary for the Ueda et al. (2003) HXLF to be in agreement with the XRB spectrum and the local Compton thick AGN space density (Draper & Ballantyne 2009, 2010; Ballantyne et al. 2011). The unabsorbed type 1 sources are evenly distributed over column densities $\log N_H = 20.0, 20.5, 21.0$, and 21.5. The Compton thin type 2 sources are distributed equally over $\log N_H = 22.0, 22.5, 23.0$, and 23.5. The contribution of Compton thick AGN to the XRB is included. To do so, it is assumed that Compton thick sources evolve similarly to less obscured AGN and are evenly distributed over $\log N_H = 24.0, 24.5$, and 25.0.

The AGN number counts in the 2–10 keV and 15–55 keV bands are also calculated. This is done by using the same AGN spectra, f_2, and f_{CT} as in the XRB model described above, including the contribution of Compton thick AGN, and by using the HXLF calculated as in Section 3.1.

3.4. Summary of Free Parameters

The light curve fitting parameters— t_0, which is related to the AGN lifetime, η, which is related to the peak Eddington ratio, and β, which determines the slope of the light curve— are determined by comparing the resulting models against the observed HXLF, evolving black hole space density, XRB spectrum, and AGN number counts. The fractional rate of massive galaxies which are triggered by secular processes each Gyr, f_{sec}, is also determined by comparing against observational constraints.

The focus of this study is not to fit the AGN light curve parameters, but to investigate the contribution to the AGN population of AGN triggered by major mergers and AGN

triggered by secular processes. Therefore, a minimization algorithm is not used. Instead, the best fit parameters for the AGN light curve are determined by considering models with $t_0 = 1.0 \times 10^7$, 5.0×10^7, 1.0×10^8, 2.5×10^8, 5.0×10^8, 7.5×10^8, and 1.0×10^9 yrs. Hopkins & Hernquist (2006) found that their model results were not very dependent on η, so the values $\eta = 0.2$, 0.4, 1.0, 2.5, and 3.0 are considered. Steps of 0.05 in the range from 0.05 to 1.0 are used to determine β. For f_{sec} the values 0.0, 0.005, 0.01, 0.02, and 0.05 Gyr^{-1} are investigated. The best fit parameters for each model are determined by minimizing a χ^2 test which takes into account the 127 HXLF data points for $z = 2.3$, 1.2, 0.6, 0.3, and 0.1 presented by Ueda et al. (2003), La Franca et al. (2005), Silverman et al. (2008), Aird et al. (2010), and Ueda et al. (2011). By comparing against the observed AGN HXLF, black hole mass density, XRB spectrum, and AGN number counts, the model is fully constrained, allowing for some conclusions to be reached about the AGN light curve parameters. The model sensitivity to the light curve parameters is discussed in Section 6.1.

4. One Population

4.1. Major Merger Triggered Quasars

First, it is assumed that all AGN are triggered by major mergers, thus, $f_{sec} = 0.0$. The best fit to the HXLF is found using the Merloni & Heinz (2008) ABHMF with the Labita et al. (2009) evolution, $t_0 = 2.5 \times 10^8$ yrs, $\beta = 0.7$, and $\eta = 2.5$, similar to that found by Cao (2010). When compared to the 127 data points from the Ueda et al. (2003), La Franca et al. (2005), Silverman et al. (2008), Aird et al. (2010), and Ueda et al. (2011) observed HXLFs in the 5 redshift ranges considered, this model has a reduced χ^2, $\chi^2_{red} = 2.4$. If t_0 is changed by 0.5×10^8 yrs, β is changed by 0.05, or η is changed by 0.5, the resulting χ^2_{red} will increase by $\sim 0.1 - 0.2$. The light curve fitting parameters are summarized in Table 1. As shown by the dot-dashed red lines in Figure 1, this model provides a relatively good fit to the observed HXLF at $z \gtrsim 1$; however, at $z < 1$, this model has $\chi^2_{red} = 2.6$ for 85 data points. The space density of major mergers at $z < 1$ is too low to explain the space density of observed AGN in this redshift range. This model is in agreement with the observed local black hole mass density (Shankar et al. 2009) and the $z \sim 2$ observed black hole mass density (Treister et al. 2010b). However, this model significantly under-predicts the XRB spectrum as well as the 2–10 keV and 15–55 keV AGN number counts. Thus, despite major merger triggered AGN being able to account for the integrated black hole growth, merger triggered AGN cannot account for the space density of the entire AGN population. Specifically, major mergers cannot account for the $z \lesssim 1$ AGN population.

The finding that major mergers are not capable of accounting for the $z \lesssim 1$ AGN

population is robust against several assumptions. To test the dependence of the merger triggered AGN only model on the SMF, the $z = 1.3$–3 SMF presented by Marchesini et al. (2009) and the $z = 0.1$ SMF presented by Cole et al. (2001) are used to define an evolving SMF. When using the combined Cole et al. (2001) and Marchesini et al. (2009) SMF, the merger triggered AGN only model is not able to account for the space density of AGN at $z \lesssim 1$, with minimum $\chi^2_{red} = 3.6$. Similarly, if the minimum mass of a potential AGN host galaxy (M_*^{min}) is reduced, the merger only model cannot supply a decent fit to the observational constraints.

4.2. Secularly Triggered AGN

Next, we consider the scenario where all AGN are triggered by secular processes. For this model, the best fit to the HXLF is found when using the Netzer (2009) ABHMF with the continuity equation evolution, $t_0 = 2.5 \times 10^8$ yrs, $\beta = 0.8$, $\eta = 0.4$, and $f_{sec} = 0.02$ Gyr^{-1}. This model has $\chi^2_{red} = 2.1$ for 127 data points. If t_0 is changed by $\sim 0.5 \times 10^8$ yrs, β is changed by 0.05, or f_{sec} is changed by 0.01 Gyr^{-1}, the resulting χ^2_{red} will change by ~ 0.2. If η is changed by ~ 0.5 the resulting χ^2_{red} will increase by ~ 0.1. As shown by the blue dashed lines in Figure 1, this model under-predicts the space density of low L_X AGN at $z \lesssim 1$ and under-predicts high L_X sources at $z \gtrsim 1$. Furthermore, this model significantly under-predicts the local black hole mass density, the XRB, and the 2–10 keV number counts. This model slightly over-predicts the *Swift*/BAT 15–55 keV number count and is inconsistent with the findings of Koss et al. (2010) that $\sim$20% of *Swift*/BAT AGN host galaxies have disturbed morphology indicative of a recent major merger. Thus, secular processes alone are not sufficient to account for the entire AGN population. Specifically, secular processes are not able to account for the AGN population at $z \gtrsim 0.5$. When the minimum mass of a potential AGN host galaxy is reduced or the evolving SMF defined by combining the Cole et al. (2001) and Marchesini et al. (2009) SMFs is used, the secular evolution only model still cannot account for the $z \gtrsim 0.5$ AGN population, with minimum $\chi^2_{red} = 2.0$. It is found that AGN triggered by secular mechanisms alone cannot explain the observed AGN population.

Neither merger triggered AGN nor secularly triggered AGN alone are able to account for the entire AGN population. Reducing the minimum mass of potential AGN host galaxies and using the combined Cole et al. (2001) and Moretti et al. (2009) SMF does not change this result. The space density of major mergers at $z < 1$ is too low to account for the low redshift AGN population but can account for the local space density of black holes. In contrast, AGN triggered by secular mechanisms are not able to account for the build up of

the black hole mass density over cosmic time. Thus, we consider the possibility that AGN are triggered by both major mergers and secular processes.

5. Two Populations

As neither the major merger triggered AGN nor the secularly triggered AGN can alone account for the entire AGN population, we now consider a two population model in which AGN are assumed to be triggered by both secular processes and major mergers. First, the major merger triggered AGN light curve is determined by finding the lowest χ^2 fit to the z = 2.3 HXLF using only the major merger triggered portion of the AGN population. Thus, the maximum possible contribution from major mergers is assumed[5]. The light curve of the secularly triggered AGN is constrained by the minimum total χ^2 fit to all 127 HXLF data points. Both the Merloni & Heinz (2008) and Netzer (2009) ABHMFs and the Labita et al. (2009) and continuity equation (Eq. 10) ABHMF evolutions are considered. It is assumed that merger triggered and secularly triggered AGN may have different light curves; thus, the light curve parameters for AGN triggered by mergers and AGN triggered by secular processes are considered separately.

We started by attempting to model both the AGN triggered by major mergers and AGN triggered by secular processes using the same ABHMF and evolution for both populations of AGN. The best fit parameters for these models are summarized by the middle section of Table 1. Despite these models providing decent fits to the observed HXLF data points, the models were not in agreement with the other observational constraints, as summarized by the middle section of Table 2. However, this exercise did demonstrate that the $z \lesssim 0.5$ AGN population is fairly well described using the Netzer (2009) ABHMF with the continuity equation evolution (Eq. 10) and the $z \gtrsim 1$ AGN population can be described by using the Merloni & Heinz (2008) ABHMF with the Labita et al. (2009) evolution. Therefore, a mixed ABHMF and evolution model was investigated.

Since the Netzer (2009) ABHMF with continuity equation evolution works well at low redshift, where secular evolution is expected to dominate, and the Merloni & Heinz (2008) ABHMF with Labita et al. (2009) evolution works well at high redshift, where major merger triggered AGN are expected to dominate, a hybrid model is calculated. Using the Merloni & Heinz (2008) ABHMF with the Labita et al. (2009) evolution, the best fit parameters for the merger triggered AGN in this model are $t_0 = 2.5 \times 10^8$ yrs, $\beta = 0.7$, and η

---

[5]If the maximum contribution from secularly triggered AGN is assumed, an appropriate fit to the HXLF can be found ($\chi^2_{red} = 1.7$), but this model cannot account for the observed local black hole mass density.

= 2.5. Using the Netzer (2009) ABHMF with the continuity equation evolution (Eq. 10), the AGN triggered by secular mechanisms are best described by the parameters $t_0 = 2.5 \times 10^8$ yrs, $\beta = 0.8$, $\eta = 0.4$, and $f_{sec} = 0.01$ Gyr^{-1}. This model does moderately well at describing the AGN HXLF, with $\chi^2_{red} = 1.4$, as shown in Figure 2. Also, this model is in agreement with the local black hole mass density observed by Shankar et al. (2009) and the $z \sim 2$ black hole mass density observed by Treister et al. (2010b), which, as shown in Figure 3, is dominated by black hole growth triggered by major mergers. Figure 4 shows that this model is also in agreement with the observed XRB spectrum. The mixed ABHMF model is in decent agreement with the 2–10 keV AGN number counts as shown in Figure 5. Figure 6 shows that the mixed ABHMF model is in good agreement with the *Swift*/BAT 15–55 keV AGN number count observed by Ajello et al. (2009). Furthermore, at the *Swift*/BAT survey flux limit of 7.6×10^{-12} erg cm^{-2} s^{-1}, we find that merger triggered AGN account for $\sim 20\%$ of 15–55 keV number count, in agreement with the findings of Koss et al. (2010). Thus, this mixed ABHMF model provides the best overall fit to the observational constraints.

The largest discrepancy between the mixed ABHMF model and the observational constraints, is the HXLF at $L_X \lesssim 10^{42}$ erg s^{-1}, specifically at $z = 0.6$. Due to the tendril nature of cosmic structure, narrow fields, which tend to provide the high z, low L_X AGN detections, will observe over dense regions when one of these tendrils passes through the observed field. This cosmic variance may cause the number counts and HXLFs observed in different fields to vary slightly (Brandt & Hasinger 2005). Observations of AGN with $L_X \lesssim 10^{42}$ erg s^{-1} and $z \sim 0.6$ can only be conducted in the *Chandra* deep fields, which are known to have significant field-to-field variation (Cowie et al. 2002). As the slope of the low L_X end of the HXLF is still fairly uncertain, cosmic variance is most likely to affect the low L_X end of the observed HXLF.

When both merger triggered and secularly triggered AGN are considered, models which use the Netzer (2009) ABHMF are in agreement with observations at $z < 0.5$, but not at high redshift. In contrast, models which use the Merloni & Heinz (2008) ABHMF for both merger and secularly triggered AGN over-predict the black hole mass density. In order to explain both high and low redshift observations, it is necessary that merger triggered and secularly triggered AGN have different ABHMFs which evolve differently with redshift. The mass distribution of black holes triggered by secular processes is, therefore, intrinsically different than the mass distribution of black holes triggered by mergers, in agreement with the findings of Schawinski et al. (2010b).

6. Discussion

An observationally based AGN triggering rate and a theoretical AGN light curve is used to model the AGN population. By considering the HXLF at five different redshifts, the black hole mass density, the XRB spectrum, and the AGN number counts in the 2–10 and 15–55 keV bands, it is determined that neither merger triggered AGN nor AGN triggered by secular processes can alone account for the entire AGN population. Two populations are necessary to describe the observed evolution and space density of AGN. Furthermore, it is found that the ABHMF of merger triggered AGN evolves more rapidly and has a higher average black hole mass than the ABHMF of secularly triggered AGN.

6.1. AGN Light Curve Model

The AGN light curve model used has three parameters, t_0, β, and η. The η parameter is related to the peak Eddington ratio of the light curve. The AGN population model is least sensitive to η, however, it is found that $\eta \gtrsim 1.0$ provides the best fit to the observational constraints, suggesting that short periods of super-Eddington accretion are likely in a significant fraction of the AGN population. The AGN population model is moderately dependent on the time scale parameter, t_0. If this time scale is too short, the AGN fade too quickly, and the space density of low luminosity AGN is severely under-predicted. Thus, t_0 is most important for the normalization of the AGN HXLF. The shape of the HXLF is primarily controlled by the slope of the light curve, which is controlled by the β parameter. The AGN population model is most sensitive to β. Changing β by 0.1 can cause the resulting HXLF shape to change substantially. The primary goal of this study is to investigate if it is necessary that AGN be triggered by both mergers and secular processes or if a single mechanism can account for the entire AGN population, not to determine the best fit AGN light curve parameters. However, the observational constraints used in this study do provide interesting restrictions on the AGN light curve parameters.

Hopkins & Hernquist (2009) point out that different models of the AGN light curve predict different light curve slopes, β. Therefore, the AGN light curve fit provides information about the physical conditions in the vicinity of the accretion disk. For example, self-regulated models, where the black hole accretion is feedback limited, predict $\beta = 0.3 - 0.8$. Meanwhile, if AGN are fueled by mass loss from a nuclear star cluster, $\beta = 0.9 - 1.0$. Models in which the fuel supply of a Shakura & Sunyaev (1973) accretion disk is suddenly cut off, predict $\beta = 0.80 - 0.84$. In all of the best fit merger triggered AGN models presented here, $\beta = 0.7$, suggesting that for merger triggered AGN, the accretion is feedback limited. Also, for the best fit model presented here, η, the parameter related to light curve peak Eddington ratio,

is much smaller for AGN triggered by secular mechanisms than for AGN triggered by major mergers.

6.2.   Two Populations of AGN

Here, it is assumed that every major merger triggers an AGN and major mergers can account for the AGN population at $z = 2.3$, thus this analysis is an upper limit for the contribution of major merger triggered AGN. Still, it is found that at $z \lesssim 2$, a significant fraction of all AGN are triggered through secular mechanisms. Figure 7 shows the space and luminosity density of AGN with $\log L_X > 42$, 43, and 44, which are triggered by mergers and secular processes as a function of redshift for the mixed ABHMF model. At all three luminosity ranges, the luminosity density and space density of AGN is dominated by major merger triggered AGN at $z \gtrsim 1.5$ and secularly triggered AGN at $z \lesssim 1.5$. By varying model parameters, we find the minimum redshift at which major mergers can dominate AGN trigger is $z \sim 1$. This finding is in agreement with Georgakakis et al. (2009), who found that $\sim$30% of the AGN space density and $\sim$25% of the AGN luminosity density at $z \sim 1$ is due to AGN hosted by disk dominated hosts, implying that secular processes are responsible for at least one quarter of the AGN luminosity density at $z \sim 1$. It is found that merger triggered AGN account for $\sim$20% of the space density of $\log L_X > 43$ AGN at $z < 0.05$, consistent with findings of Koss et al. (2010). Thus, AGN hosted by disk dominated galaxies are a significant fraction of the AGN population by $z \sim 1$, indicating that secular evolution is an important mode of galaxy evolution at this redshift.

Similarly, Draper & Ballantyne (2011b) found that for AGN at $z \lesssim 1$ the host galaxies of obscured and unobscured AGN are, on average, the same, suggesting that at $z \lesssim 1$ AGN and galaxy evolution is controlled by secular processes. However, at $z \gtrsim 1$, the host galaxies of unobscured AGN are intrinsically less dusty than the host galaxies of obscured AGN at similar redshifts, suggesting a fundamental change in the mechanisms which control AGN activity at $z \sim 1$ (Draper & Ballantyne 2011b). Indeed, Figure 2 shows that, at $z \lesssim 1$, AGN triggered through secular processes dominate even the high L_X end of the HXLF, while fading major merger triggered AGN dominate the low L_X end of the HXLF. These findings are also in agreement with the conclusions of a variety of recent observational studies which found that secular processes are an important form, and possibly the dominate form, of galaxy evolution at $z \lesssim 2$ (Georgakakis et al. 2009; Allevato et al. 2011; Cisternas et al. 2011; Schawinski et al. 2011; Williams et al. 2011). Indeed, according to the HXLF, we find that AGN triggered by secular processes can account for the entire AGN population with $\log L_X > 43$ at $z \lesssim 0.5$. Hopkins & Hernquist (2006) suggest that secularly triggered AGN

are not cosmologically important; however, the findings of this study illustrate that AGN triggered by secular mechanisms are necessary to describe the AGN population and dominate the space density of AGN with $\log L_X > 43$ at $z \lesssim 1.5$.

The findings of Schawinski et al. (2010b) suggest that this fundamental change in AGN activity at $z \sim 1.5$ is due to cosmic downsizing. By studying AGN black hole masses as a function of host galaxy morphology for AGN observed by the Sloan Digital Sky Survey (SDSS), Schawinski et al. (2010b) find that it is preferentially the least massive black holes in less massive early type galaxies (stellar mass $M_* \sim 10^{10}$ $M_\odot$) which are currently active. In contrast, the black holes which are currently active in late type galaxies are preferentially the most massive black holes hosted by more massive late type host galaxies ($M_* \sim 10^{11}$ $M_\odot$). A stellar disk generally indicates that a galaxy has not undergone a major merger or that the last major merger experienced by the galaxy was long enough ago that a disk had time to reform, $\gtrsim 500$ Myr (Hota et al. 2011). We can therefore assume that, for AGN hosted by late type galaxies, the current episode of AGN activity was triggered by secular processes. Schawinski et al. (2010b) suggest that the early type galaxy hosts in their sample may be smaller versions of the mode of galaxy evolution experienced by massive ellipticals at high redshift. Thus, the early type host galaxies in the sample of Schawinski et al. (2010b) may host downsized versions of major merger triggered AGN. Thus, it appears that the dominance of major mergers in galaxy evolution began to decline by $z \sim 2$ and is continuing to decline, in agreement with the theory of cosmic downsizing. Meanwhile, the importance of secular evolution increased as the importance of major mergers decreased, until secular evolution became the dominate form of galaxy evolution at $z \sim 1.5$. Since we are still early in the era of secularly dominated galaxy evolution, it is the more massive systems which are currently undergoing secularly triggered AGN activity. Cosmic downsizing would therefore predict that as the era of secular dominance continues, AGN triggered through secular processes will become more common in lower mass systems.

6.3. ABHMF and Evolution

It is found that AGN triggered by major mergers at $z < 4$ have, on average, more massive central black holes than AGN triggered by secular processes, at least at high redshift. Locally, it appears that merger triggered AGN and secularly triggered AGN have similar black holes masses (Schawinski et al. 2010b), necessitating that the ABHMF of merger triggered AGN evolves differently than the ABHMF of secularly triggered AGN. The ABHMF of AGN triggered by secular mechanisms appears to evolve in a manner consistent with the continuity equation (Eq. 10), which describes the evolution of the combined active and quiescent black

hole mass function (e.g., Small & Blandford 1992; Merloni & Heinz 2008). However, if the ABHMF of merger triggered AGN evolves following the continuity equation, then at $z \gtrsim 1$ the average active black hole mass is too small to account for the high L_X end of the HXLF. In contrast, if the Labita et al. (2009) ABHMF evolution is used to evolve the ABHMF of secularly triggered AGN, then the low L_X end of the $z \lesssim 1$ HXLF is significantly under-predicted. Thus, it appears that not only are both secular processes and major mergers important mechanisms for triggering the $z < 2$ AGN population, but these two mechanisms trigger different populations of black holes and these two populations have different redshift evolution.

It is not surprising that the ABHMF of merger triggered AGN evolves differently from the secularly triggered ABHMF and the quiescent black hole mass function. The major merger rate evolves strongly with redshift and galaxy mass (Hopkins et al. 2010a). Thus, it is expected that the ABHMF of AGN triggered by major mergers would also evolve strongly with redshift (e.g., Treister et al. 2011). In contrast, the rate of AGN being triggered by secular evolution, f_{sec}, is assumed to be constant with redshift. Therefore, it is expected that the ABHMF for AGN triggered by secular processes will be less redshift dependent than the ABHMF for merger triggered AGN. Also, as the majority of supermassive black holes at any redshift are quiescent, the combined quiescent and active black hole mass function evolves more slowly with redshift than the merger triggered ABHMF. Thus, it is expected that the merger triggered ABHMF will evolve more strongly with redshift than the ABHMF of secularly triggered AGN or of the combined active and quiescent black hole mass function.

6.4. The Connection Between Compton Thick AGN and Mergers

Observational and theoretical evidence suggests that Compton thick AGN are AGN which were recently triggered by a mechanism which has caused a large amount of gas and dust to be funneled into the nuclear regions of the host galaxy (e.g., Fabian 1999; Page et al. 2004; Fabian et al. 2008, 2009; Draper & Ballantyne 2010; Treister et al. 2010a; Draper & Ballantyne 2011b). Due to the large amount of gas and dust required for the rapid AGN fueling and high column density necessary for an AGN to be Compton thick, the most likely triggering process is a wet major merger (Sanders et al. 1988; Hopkins et al. 2006a), though Weinzirl et al. (2011) argue that Compton thick levels of obscuration are also possible in instances of clumpy cold-flow accretion onto the host galaxy. Here, we set f_{CT} = 0.0 for the secularly triggered AGN and calculate f_{CT} for the merger triggered AGN as described in Section 3.1. If it is assumed that Compton thickness is an evolutionary phase which only merger triggered AGN experience, the χ^2_{red} of the mixed ABHMF increases by

0.1 and the model is still in agreement with the observed black hole space density, XRB spectrum, and the 2–10 keV and 15–55 keV number counts. Therefore, the hypothesis that Compton thick AGN are an evolutionary stage of merger triggered AGN is fully consistent with the model presented here.

7. Summary

By combining an observationally motivated AGN triggering rate and a theoretically motivated AGN light curve, an AGN population synthesis model is developed which can track the evolution of AGN triggered by mergers and secular processes. The light curve parameters are constrained by comparing model predictions against the observed AGN HXLF. The observed space density of supermassive black holes, AGN number counts, and XRB spectrum are also considered. The results of this study are summarized below.

• Neither AGN triggered by major mergers nor AGN triggered by secular mechanisms alone are capable of accounting for the entire observed AGN population at $z \lesssim 2$. This finding is independent of the SMF used or the potential AGN host galaxy minimum mass.

• The dominant AGN triggering mechanism switches from major mergers at $z \gtrsim 1.5$ to secular mechanisms by $z \sim 1$. This is a natural consequence of both the major merger rate and fraction of gas rich galaxies increasing with redshift. However, both major mergers and secular processes are important triggering mechanisms for AGN over the entire redshift range considered, especially at moderate luminosities. .

• The black hole mass density is dominated by black hole growth triggered by major mergers over the entire redshift range considered.

• The space density and luminosity density of AGN with $\log L_X >$ 42, 43, and 44 is dominated by AGN triggered by major mergers at $z \gtrsim 1.5$ and by AGN triggered by secular processes at $z \lesssim 1.5$.

• The XRB is dominated by emission from AGN triggered by secular mechanisms.

• The ABHMF of AGN triggered by major mergers is different from the ABHMF of AGN triggered by secular mechanisms. At high redshift, the average black hole triggered by major mergers is more massive than the average black hole triggered by secular processes, which is consistent with cosmic downsizing.

• The evolution of the ABHMF of AGN triggered by major mergers is also different from the evolution of the ABHMF of AGN triggered through secular mechanisms, with

the ABHMF of major merger triggered AGN evolving more rapidly with redshift than the ABHMF of AGN triggered by secular processes. The observed evolution of Labita et al. (2009) appears to describe the evolution of the merger triggered AGN ABHMF well. In contrast, the continuity equation (Eq. 10) describes the evolution of the ABHMF for secularly triggered AGN. This finding is consistent with the strong redshift evolution of the major merger rate.

• The findings of this study are not changed if Compton thick AGN are an evolutionary stage only experienced by major merger triggered AGN.

REFERENCES

Ajello, M., Greiner, J., Sato, G., et al.2008, ApJ, 689, 666

Ajello, M., Costamante, L., Sambruna, R.M., et al.2009, ApJ, 699, 603

Alexander, D.M., Swinbank, A.M., Smail, I., McDermid, R., Nesvadba, N.P.H. 2010, MN-RAS, 402, 2211

Allevato, V., Finoguenov, A., Cappelluti, N., et al.2011, ApJ, 736, 99

Aird, J., Nandra, K., Laird, E.S., et al.2010, MNRAS, 401, 2531

Ballantyne, D.R., Draper, A.R., Madsen, K.K., Rigby, J.R., & Treister, E. 2011, ApJ, 736, 56

Ballantyne, D.R., Everett, J.E., Murray, N. 2006, ApJ, 639, 740

Barnes, J.E. & Hernquist, L. 1996, ApJ, 471, 115

Bertone, S., Schaye, J., Booth, C.M., et al.2010, MNRAS, 408, 1120

Bournaud, F., Dekel, A., Teyssier, R., et al.2011, ApJ, 741, L33

Brandt, W.N. & Hasinger G. 2005, ARA&A, 43, 827

Brunner, H., Cappelluti, N., Hasinger, G., et al.2008, A&A, 479, 283

Brusa, M., Fiore, F., Santini, P., et al. 2009, A&A, 507, 1277

Cao, X. 2010, ApJ, 725, 388

Cao, X. & Xu, Y.-D. 2007, MNRAS, 377, 425

Cappelluti, N., Brusa, M., Hasinger, G., et al.2009, A&A, 497, 635

Cardamone, C.N., Urry, C.M., Schawinski, K., et al.2010, ApJ, 721, L38

Carlberg, R.G., 1990, ApJ, 350, 505

Chen, Y.-M., Wang, J.-M., Yan, C.-S., Hu, C., & Zhang, S. 2009, ApJ, 695, L130

Churazov, E., Sunyaev, R., Revnivtsev, M., et al.2007, A&A, 467, 529

Cisternas, M., Jahnke, K., Inskip, K.J., et al.2011, ApJ, 726, 57

Cole, S., Norberg, P., Baugh, C.M., et al.2001, MNRAS, 326, 255

Cowie, L.L., Garmire, G.P. Bautz, M.W., et al.2002, ApJ, 566, L5

Crenshaw, D.M., Kraemer, S.B., & Gabel, J.R. 2003, AJ, 126, 1690

Dahlen, T., Mobasher, B., Dickinson, M., et al.2007, ApJ, 654, 172

Davies, R.I., Müller Sánchez, F., Genzel, R., et al.2007, ApJ, 671, 1388

De Luca, A. & Molendi, S. 2004, A&A, 419, 837

Draper, A.R. & Ballantyne, D.R., 2009, ApJ, 707, 778

Draper, A.R. & Ballantyne, D.R., 2010, ApJ, 715, L99

Draper, A.R. & Ballantyne, D.R., 2011a, ApJ, 729, 109

Draper, A.R. & Ballantyne, D.R., 2011b, ApJ, 740, 57

Elvis, M., Civano, F., Vignali, C., et al.2009, ApJS, 184, 158

Fabian, A.C. 1999, MNRAS, 308, L39

Fabian, A.C., Vasudevan, R.V., & Gandhi, P. 2008, MNRAS, 385, L43

Fabian, A.C., Vasudevan, R.V., Mushotzky, R.F., Winter, L.M., & Reynolds, C.S. 2009, MNRAS, 394, L89

Gendreau, K.C., Mushotzky, R., Fabian, A.C., et al.1995, PASJ, 47, L5

Georgakakis, A., Coil, A.L., Laird, E.S., et al.2009, MNRAS, 397, 623

Gilli, R., Comastri, A., Hasinger, G. 2007, A&A, 463, 79

Gruber, D.E., Matteson, J.L., Peterson, L.E., & Jung, G.V. 1999, ApJ, 520, 124

Hambrick, D.C., Ostriker, J.P., Naab, T., Johansson, P.H. 2011, ApJ, 738, 16

Hernquist, L. 1989, Nature, 340, 687

Hickox, R., Jones, C., Forman, W.R., et al.2009, ApJ, 696, 891

Hocuk, S. & Spaans, M. 2011, A&A, in press (arXiv:1109.6593)

Hopkins, P.F., Bundy, K., Croton, D., et al.2010a, ApJ, 715, 202

Hopkins, P.F., Croton, D., Bundy, K., et al.2010b, ApJ, 724, 915

Hopkins, P.F. & Hernquist, L. 2009, ApJ, 298, 1550

Hopkins, P.F. & Hernquist, L. 2006, ApJS, 166, 1

Hopkins, P.F., Hernquist, L., Cox, T.J., et al.2006a, ApJS, 163, 1

Hopkins, P.F., Somerville, R.S., Hernquist, L. 2006b, ApJ, 652, 864

Hota, A., Sirothia, S.K., Ohyama, Y., et al.2011, MNRAS, 417, L36

Kauffmann, G. & Haehnelt, M. 2000, MNRAS, 311, 576

Kocevski, D.D., Faber, S.M., Mozena, M., et al.2012, ApJ, 744, 148

Kormendy, J. & Kennicutt, R.C. 2004, ARA&A, 42, 603

Kormendy, J. & Richstone, D. 1995, ARA&A, 33, 581

Koss, M., Mushotzky, R., Veilleux, S., & Winter, L. 2010, ApJ, 716, L125

Kumar, P. & Johnson, J.L. 2010, MNRAS, 404, 2170

Kushino, A., Ishisaki, Y., Morita, U., et al., 2002, PASJ, 54, 327

Labita, M., Decarli, R., Treves, A., & Falomo, R. 2009, MNRAS, 399, 2099

La Franca, F., Fiore, F., Comastri, A., et al.2005, ApJ, 635, 864

Lagos, C.D.P., Cora, S.A., & Padilla, N.D. 2008, MNRAS, 388, 587

Lumb, D.H., Warwick, R.S., Page, M., & De Luca, A. 2002, A&A, 389, 93

Magorrian, J., Tremaine, S., Richstone, D., et al.1998, AJ, 115, 2285

Malizia, A., Stephen, J.B., Bassani, L., et al.2009, MNRAS, 399, 944

Marchesini, D., van Dokkum, P.G., Förster Schreiber, N.M., et al.2009, ApJ, 701, 1765

Marconi, A., Risaliti, G., Gilli, R., et al.2004, MNRAS, 351, 169

Mateos, S., Warwick, R.S., Carrera, F.J., et al.2008, A&A, 492, 51

Merloni, A. & Heinz, S. 2008, MNRAS, 308, 1011

Moretti, A., Pagani, C., Cusumano, G., et al.2009, A&A, 493, 501

Natarajan, P. & Treister, E. 2009, MNRAS, 393, 838

Netzer, H. 2009, ApJ, 695, 793

Orban de Xivry, G., Davies, R., Schartmann, M., et al.2011, MNRAS, 417, 2721

Page, M.J., Stevens, J.A., Ivison, R.J., & Carrera, F.J. 2004, ApJ, 611, L85

Pérez-González, P.G., Rieke, G.H., Villar, V., et al.2008, ApJ, 675, 234

Pierce, C.M., Lotz, J.M., Laird, E.S., et al.2007, ApJ, 660, L19

Peterson, B.M. & Bentz, M.C. 2006, New Astronomy Reviews, 50, 796

Puccetti, S., Capalbi, M., Giommi, P., et al.2011, A&A, 528, 122

Revnivtsev, M., Gilfanov, M., Sunyaev, R., Jahoda, K., & Markwardt, C., 2003, A&A, 411, 329

Ross, R.R. & Fabian, A.C. 2005, MNRAS, 358, 211

Sanders, D.B., Soifer, B.T., Elias, J.H., et al.1988, ApJ, 325, 74

Schawinski, K., Treister, E., Urry, C.M., et al.2011, ApJ, 727, L31

Schawinski, K., Dowlin, N., Thomas, D., Urry, C.M., & Edmondson, E. 2010a, ApJ, 714, L112

Schawinski, K., Urry, C.M., Virani, S., et al.2010b, ApJ, 711, 284

Schawinksi, K., Virani, S., Simmons, B., et al.2009, ApJ, 692, L19

Shakura, N.I. & Sunyaev, R.A. 1973, A&A, 24, 337

Shankar, F., Weinberg, D.H., & Miralda-Escudé, J. 2009, ApJ, 690, 20

Shen, Y. 2009, ApJ, 704, 89

Silk, J. & Rees, M.J. 1998, A&A, 331, L1

Silverman, J.D., Green, P.J., Barkhouse, W.A., et al.2008, ApJ, 679, 118

Silverman, J.D., Kampczyk, P., Jahnke, K., et al.2011, ApJ, 743, 2

Small, T.A. & Blandford, R.D. 1992, MNRAS, 259, 725

Sołtan, A. 1982, MNRAS, 200, 115

Treister, E., Natarajan, P., Sanders, D.B., et al.2010a, Science, 328, 600

Treister E., Schawinski, K., Volonteri, M., Natarajan, P., & Gawiser, E. 2011, Nature, 474, 356

Treister, E., Urry, C.M., Schawinski, K., et al.2010b, ApJ, 722, L238

Treister, E., Urry, C.M., Virani, S. 2009, ApJ, 696, 110

Treister, E. & Urry, C.M. 2006, ApJ, 652, L79

Tremaine, S., Gebhardt, K., Bender, R., et al.2002, ApJ, 574, 740

Trichas, M., Georgakakis, A., Rowan-Robinson, M., et al.2009, MNRAS, 399, 663

Türler, M., Chernyakova, M., Courvoisier, T. J.-L., et al.2010, A&A, 512, 49

Ueda, Y., Akiyama, M., Ohta, K., & Miyaji, T. 2003, ApJ, 598, 886

Ueda, Y., Hiroi, K., Isobe, N., et al.2011, PASJ, in press (arXiv:1109.0852)

Vasudevan, R.V., Mushotzky, R.F., Winter, L.M., & Fabian, A.C. 2009, MNRAS, 399, 1553

Vecchi, A., Molendi, S., Guainazzi, M., Fiore, F., & Parmar, A. 1999, A&A, 349, L73

Vittorini, V., Shankar, F. & Cavaliere, A. 2005, MNRAS, 363, 1376

Volonteri, M., Haardt, F., & Madau, P. 2003, ApJ, 582, 559

Weinzirl, T., Jogee, S., Conselice, C.J., et al.2011, ApJ, 743, 87

Williams, R.J., Quadri, R.F., & Franx, M. 2011, ApJ, 738, L25

Yamada, T., Kajisawa, M., Akiyama, M., et al.2009, ApJ, 699, 1354

Yu, Q. & Tremaine, S. 2002, MNRAS, 335, 965

Table 1.   Summary of derived model free parameters.

Model	Merger Triggered AGN			Secularly Triggered AGN			
	t_0 (yr)	β	η	t_0 (yr)	β	η	f_{sec} (Gyr^{-1})
One Population Models							
Mergers only	2.5×10^8	0.7	2.5	-	-	-	0.0
Secular only	-	-	-	2.5×10^8	0.8	0.4	0.02
Two Population Models							
N09 w/ Eq. 10	2.5×10^8	0.7	0.4	5×10^8	0.5	2.5	0.005
N09 w/ L09	1×10^8	0.5	1.0	2.5×10^8	0.6	2.5	0.005
MH08 w/ Eq. 10	2.5×10^8	0.8	2.5	5×10^8	0.7	2.5	0.01
MH08 w/ L09	2.5×10^8	0.7	2.5	5×10^8	0.8	2.5	0.005
Two Population Mixed ABHMF Model							
Mixed ABHMF	2.5×10^8	0.7	2.5	2.5×10^8	0.8	2.5	0.01

Note. — MH08 refers to the Merloni & Heinz (2008) ABHMF, N09 refers to the Netzer (2009) ABHMF, and L09 refers to the Labita et al. (2009) ABHMF evolution. The mixed ABHMF model uses the MH08 ABHMF with L09 evolution for the merger triggered AGN and the N09 ABHMF with the continuity equation (Eq. 10) evolution for the secularly triggered AGN.

Table 2.   Summary of model fits to the observational constraints.

Model	d.o.f.[a]	χ^2_{red}[b]	$\rho_\bullet$[c]	XRB[d]	2–10 keV[e]	15–55 keV[f]
One Population Models						
Mergers only	123	2.4	$\checkmark$	$\times$	$\times$	$\times$
Secular only	122	2.1	$\times$	$\times$	$\times$	$\times$
Two Population Models						
N09 w/ Eq. 10	119	1.5	$\times$	$\times$	$\checkmark$	$\checkmark$
N09 w/ L09	119	1.4	$\times$	$\times$	$\checkmark$	$\checkmark$
MH08 w/ Eq. 10	119	1.7	$\times$	$\times$	$\times$	$\times$
MH08 w/ L09	119	1.5	$\checkmark$	$\times$	$\times$	$\times$
Two Population Mixed ABHMF Model						
Mixed ABHMF[g]	119	1.4	$\checkmark$	$\checkmark$	$\checkmark$	$\checkmark$

[a]The number of degrees of freedom for the χ^2 test reported in column χ^2_{red}.

[b]The quoted χ^2_{red} refers to the 127 HXLF data points plotted in Figure 1.

[c]A $\times$ in this column denotes that, when considering the two black hole space density data points, $\chi^2 > 4.0$ for the designated model.

[d]A $\times$ in this column denotes that this model either over or under-predicts the XRB by more than 25% in the 10–50 keV band.

[e]A $\times$ in this column denotes that, this model either over or under-predicts the the 2–10 keV observed number counts shown in Figure 5 by more than 25% at all fluxes.

[f]A $\times$ in this column denotes that, this model either over or under-predicts the 15–55 keV observed $\log N$–$\log S$ shown in Figure 6 by more than 25% at all fluxes.

[g]The mixed ABHMF model uses the MH08 ABHMF with L09 evolution for the merger triggered

AGN and the N09 ABHMF with the continuity equation (Eq. 10) evolution for the secularly triggered AGN.
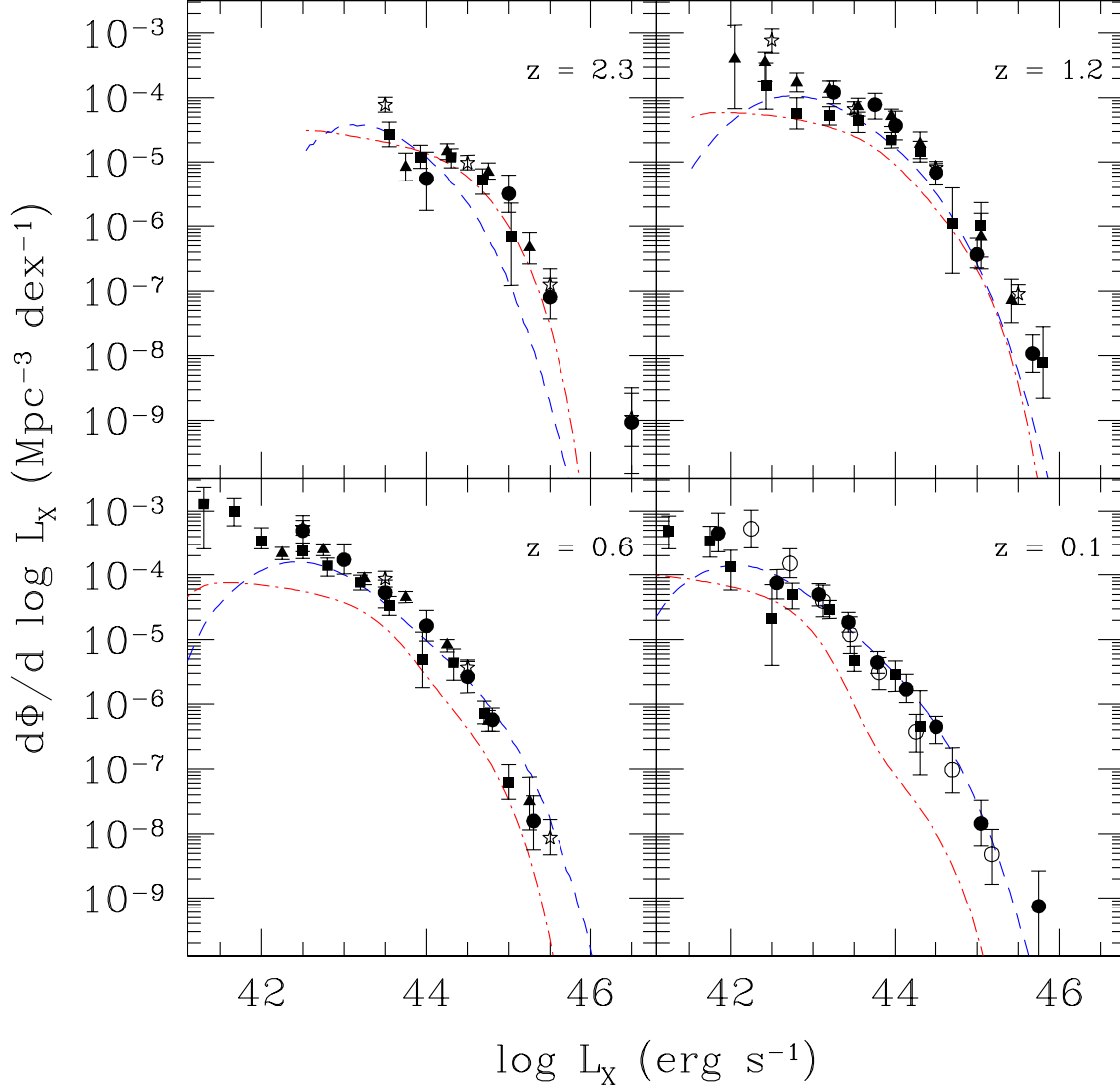
Fig. 1.— Best fit one population models compared against the observed HXLF. The dot-dashed red lines show the HXLF from the best fit major merger trigger only model and the dashed blue lines show the HXLF from the best fit secular processes trigger only model. The data points show measurements of the HXLF by Ueda et al. (2003; filled circles), La Franca et al. (2005; stars), Silverman et al. (2008; triangles), Aird et al. (2010; squares), and Ueda et al. (2011; open circles).
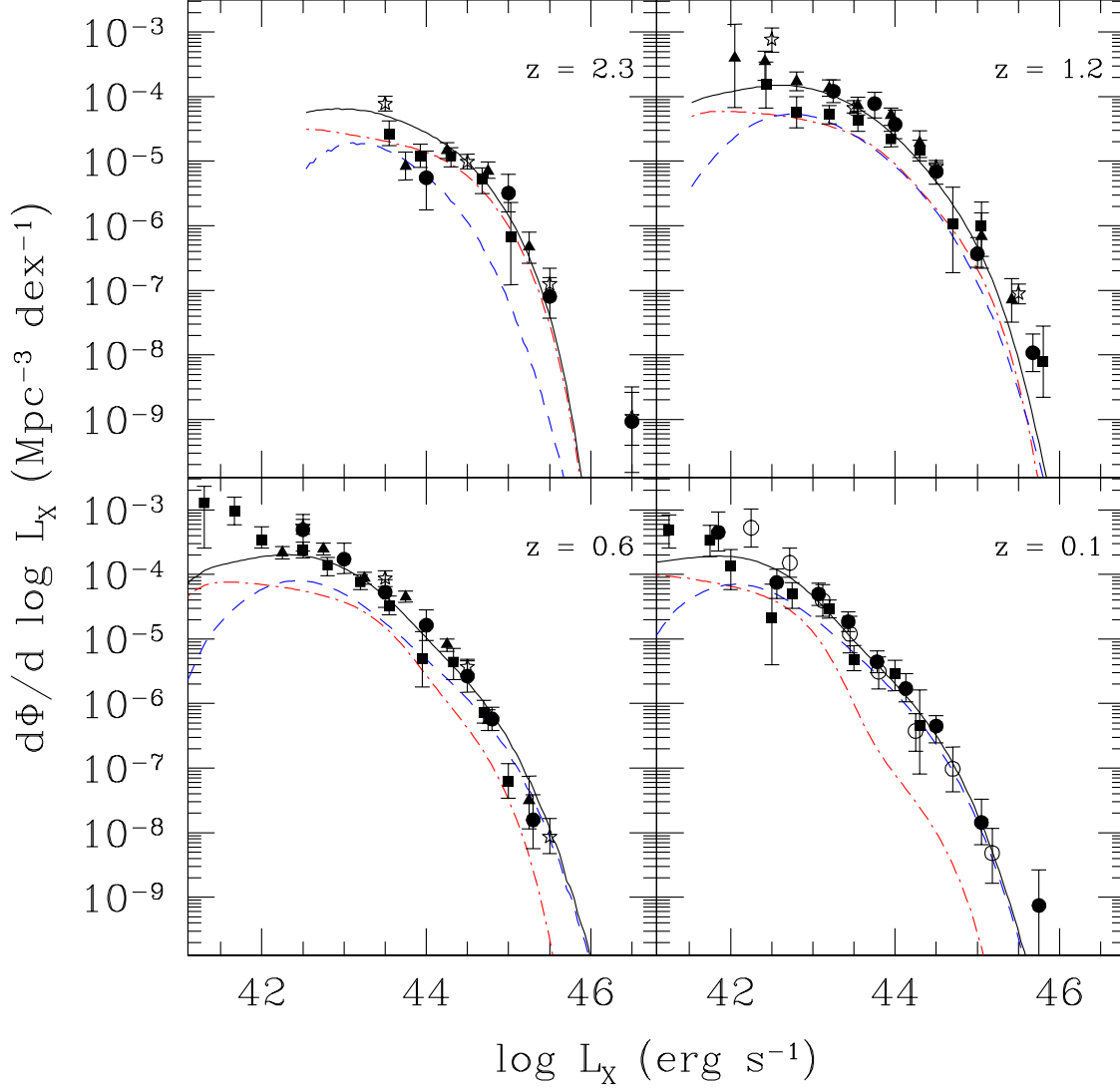
Fig. 2.— The HXLF predicted by the mixed ABHMF model, which has $\chi^2_{red} = 1.4$. The solid black line is the total AGN HXLF. The dot-dashed red lines show the contributions from AGN triggered by mergers and the dashed blue lines show the contribution from AGN triggered by secular mechanisms. The data points are the same as in Figure 1.
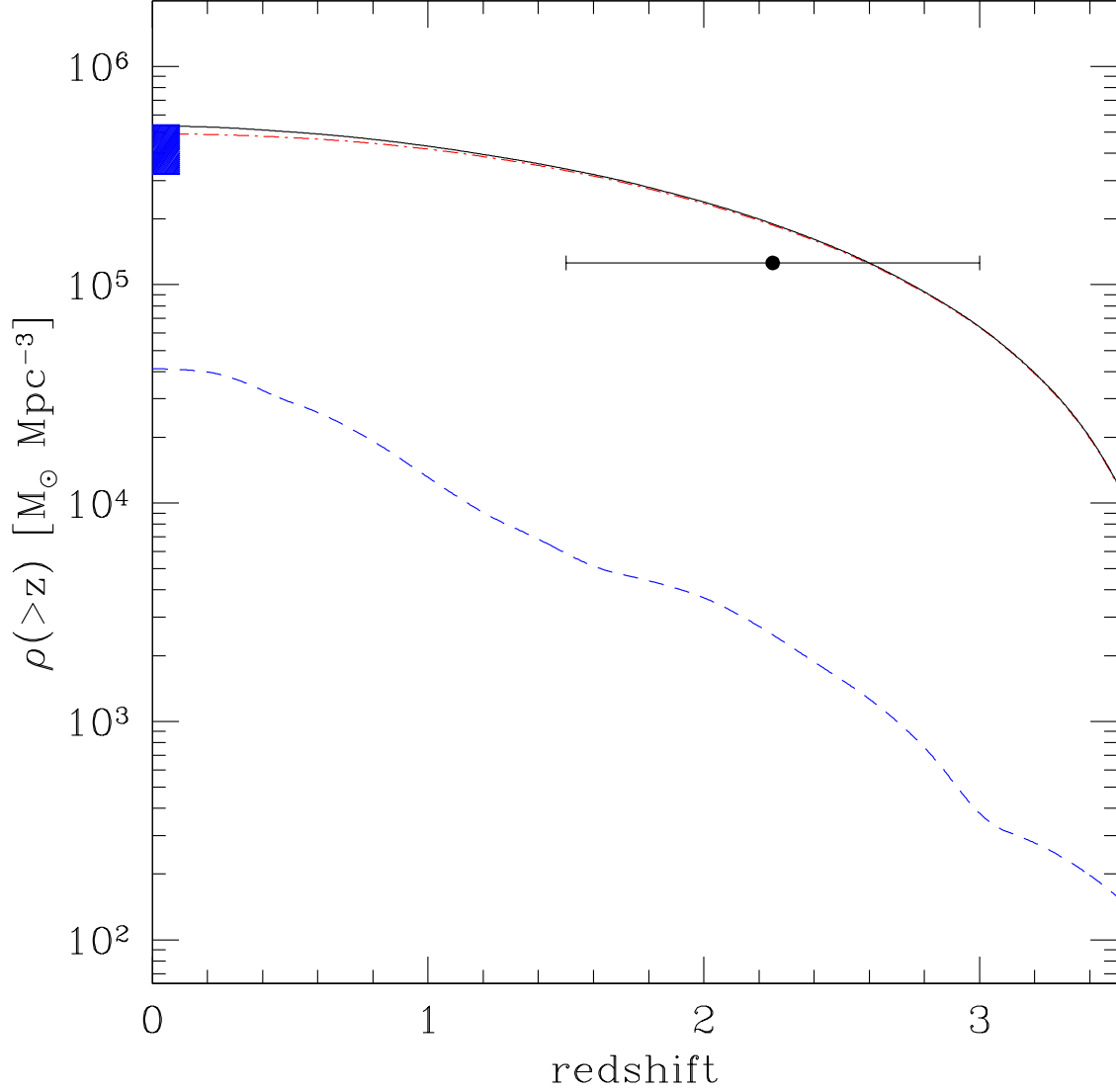
Fig. 3.— The black hole mass density with respect to redshift, predicted by the mixed ABHMF model. The line styles are the same as in Figure 2. The $z \sim 0$ shaded region is the local black hole mass density observed by Shankar et al. (2009) and the $z \sim 2$ data point is the black hole mass density observed by Treister et al. (2010b).
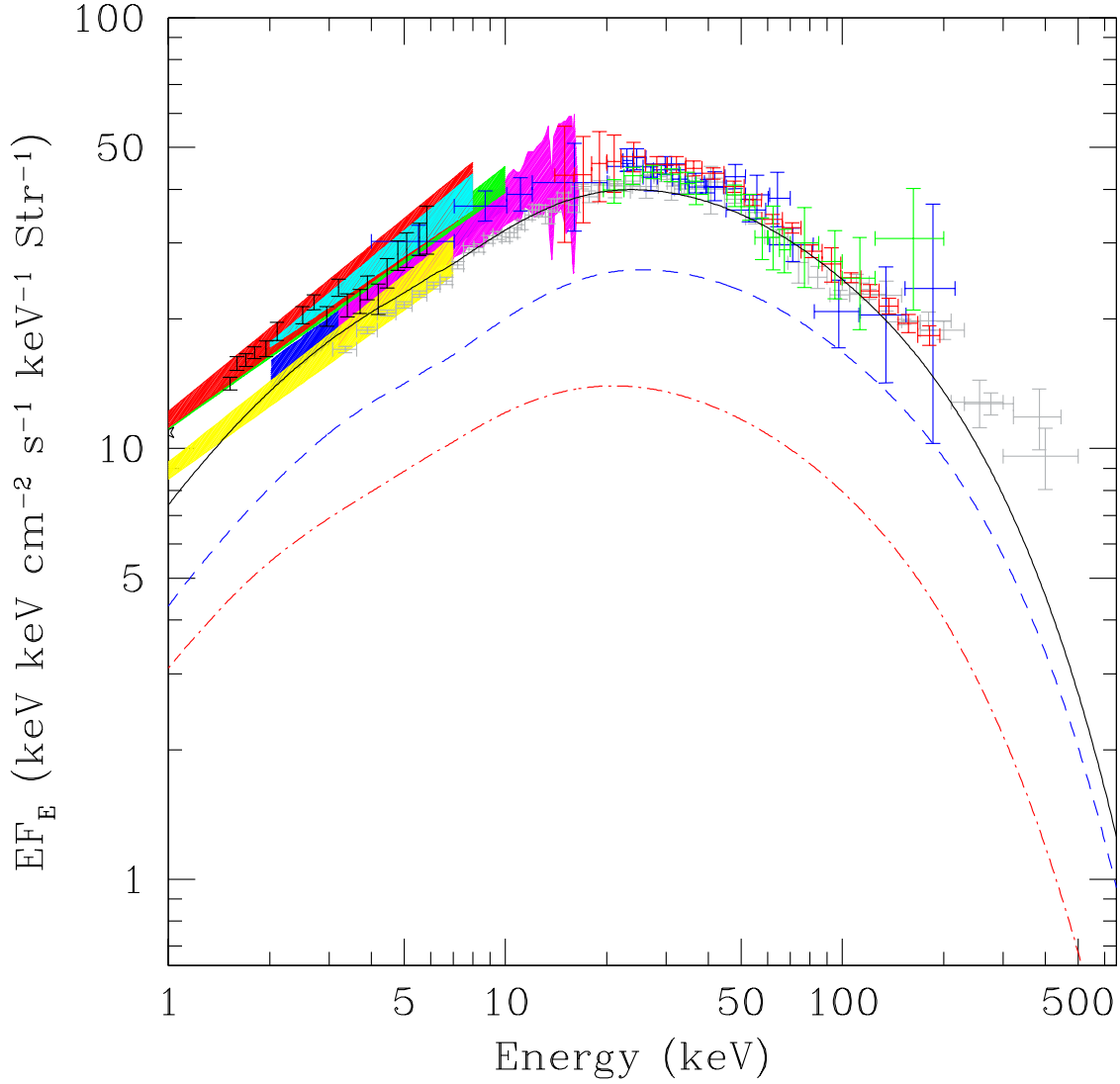
Fig. 4.— The XRB spectrum predicted by the mixed ABHMF model. The line styles are the same as in Figure 2. Colored regions and data points show measurements from various instruments; blue: *ASCA* GIS (Kushino et al. 2002); magenta: *Rossi X-ray Timing Explorer* (*RXTE*; Revnivtsev et al. 2003); green: XMM-*Newton* (Lumb et al. 2002); red: *BeppoSAX* (Vecchi et al. 1999); yellow: *ASCA SIS* (Gendreau et al. 1995); cyan: XMM-*Newton* (De Luca & Molendi 2004); grey data: *HEAO*-1 (Gruber et al. 1999); blue data: *INTEGRAL* (Churazov et al. 2007); red data: *Swift*/BAT (Ajello et al. 2008); black data: *Swift*/XRT (Moretti et al.2009); green data: *INTEGRAL* (Türler et al. 2010).
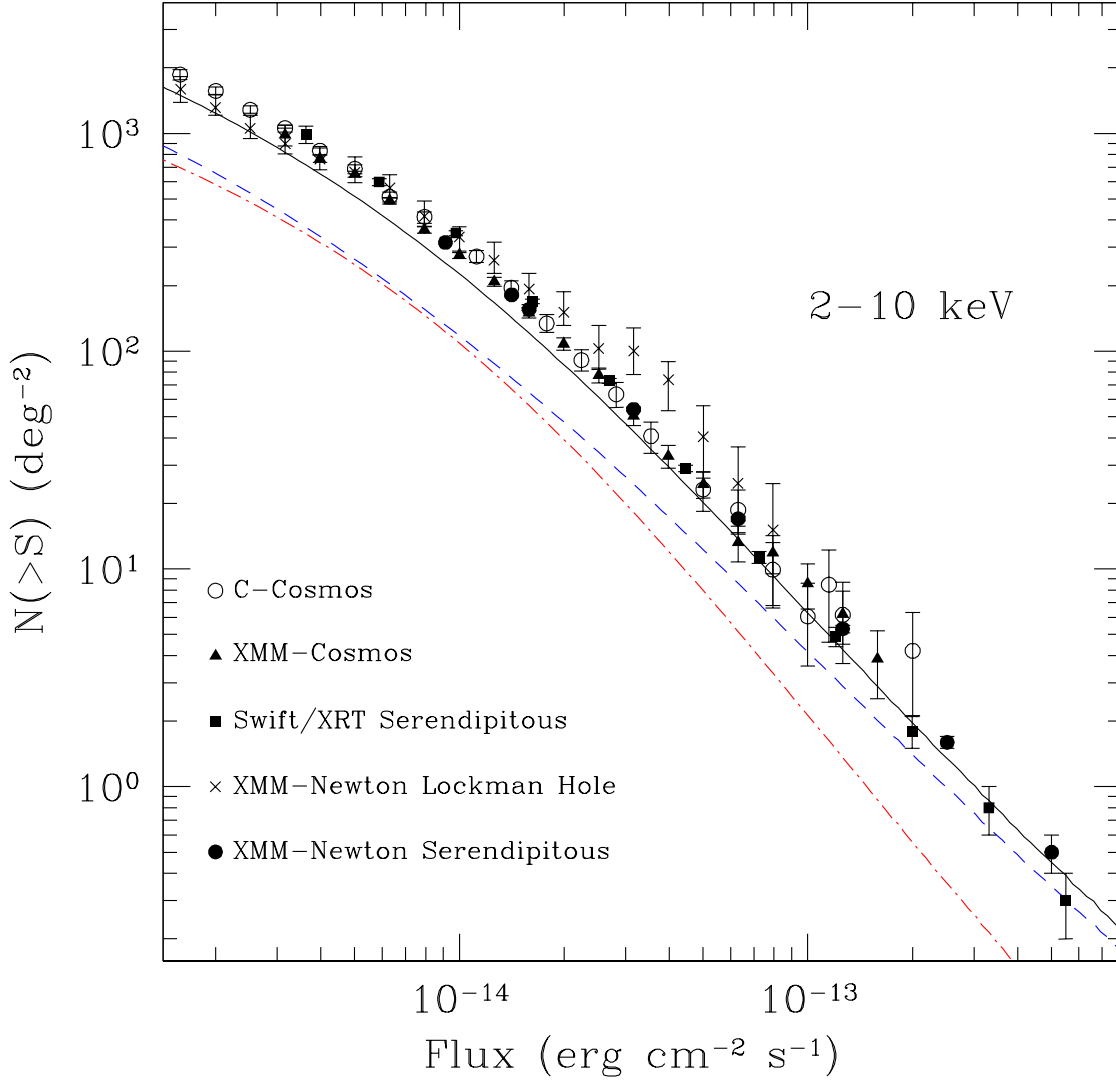
Fig. 5.— The 2–10 keV AGN $N(> S)$ predicted by the mixed ABHMF model. The line styles are the same as in Figure 2. The plotted data show observed the number counts from various surveys: C-COSMOS (Elvis et al. 2009), XMM-COSMOS (Cappelluti 2009), *Swift*/XRT Serendipitous (Puccetti et al. 2011), XMM-*Newton* Lockman Hole (Brunner et al. 2008), and XMM-*Newton* Serendipitous (Mateos et al. 2008).
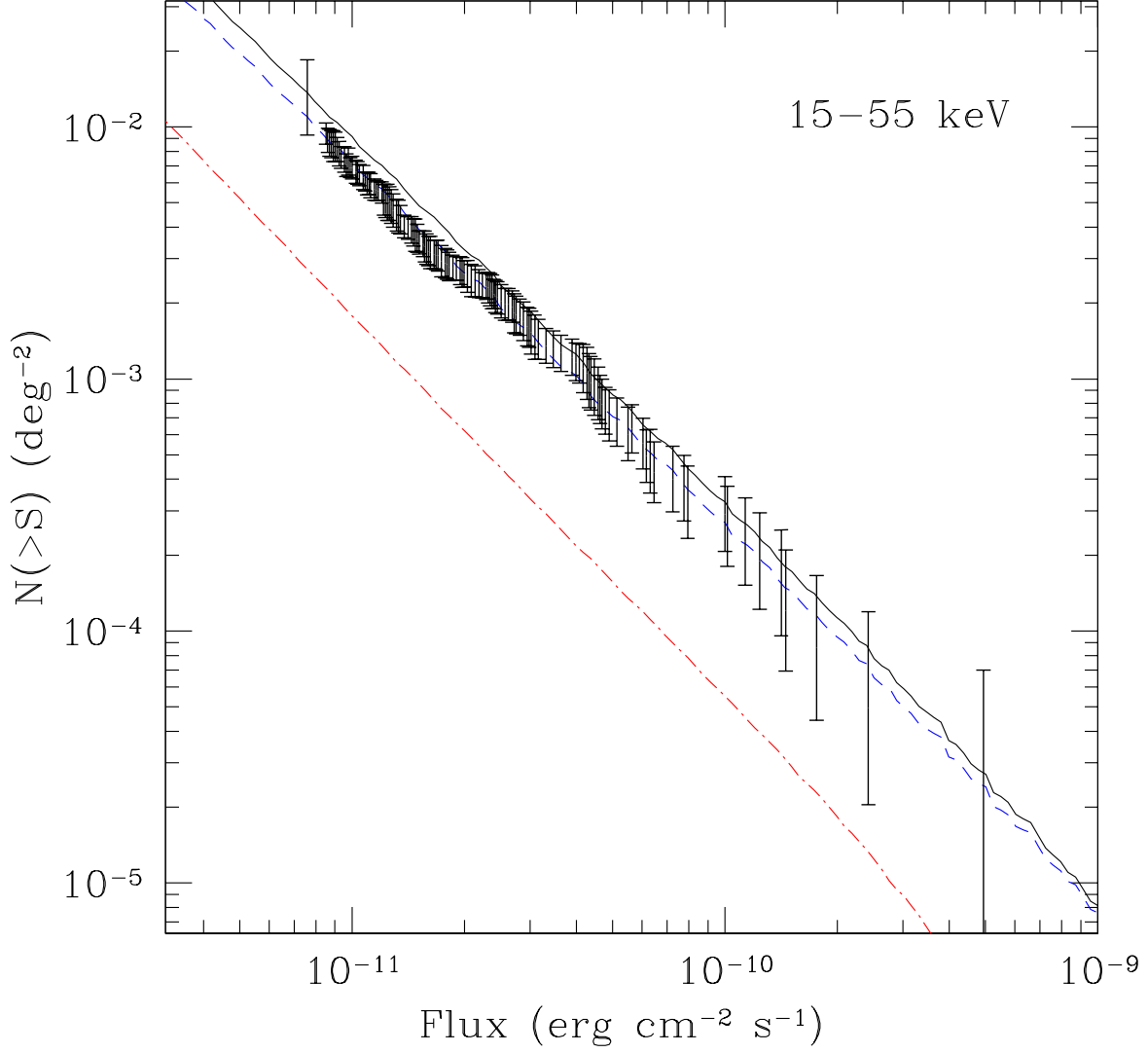
Fig. 6.— The 15–55 keV AGN $N(> S)$ predicted by the mixed ABHMF model. The line styles are the same as in Figure 2. The data points show the 15-55 keV AGN $\log N$–$\log S$ relation observed by *Swift*/BAT (Ajello et al. 2009).
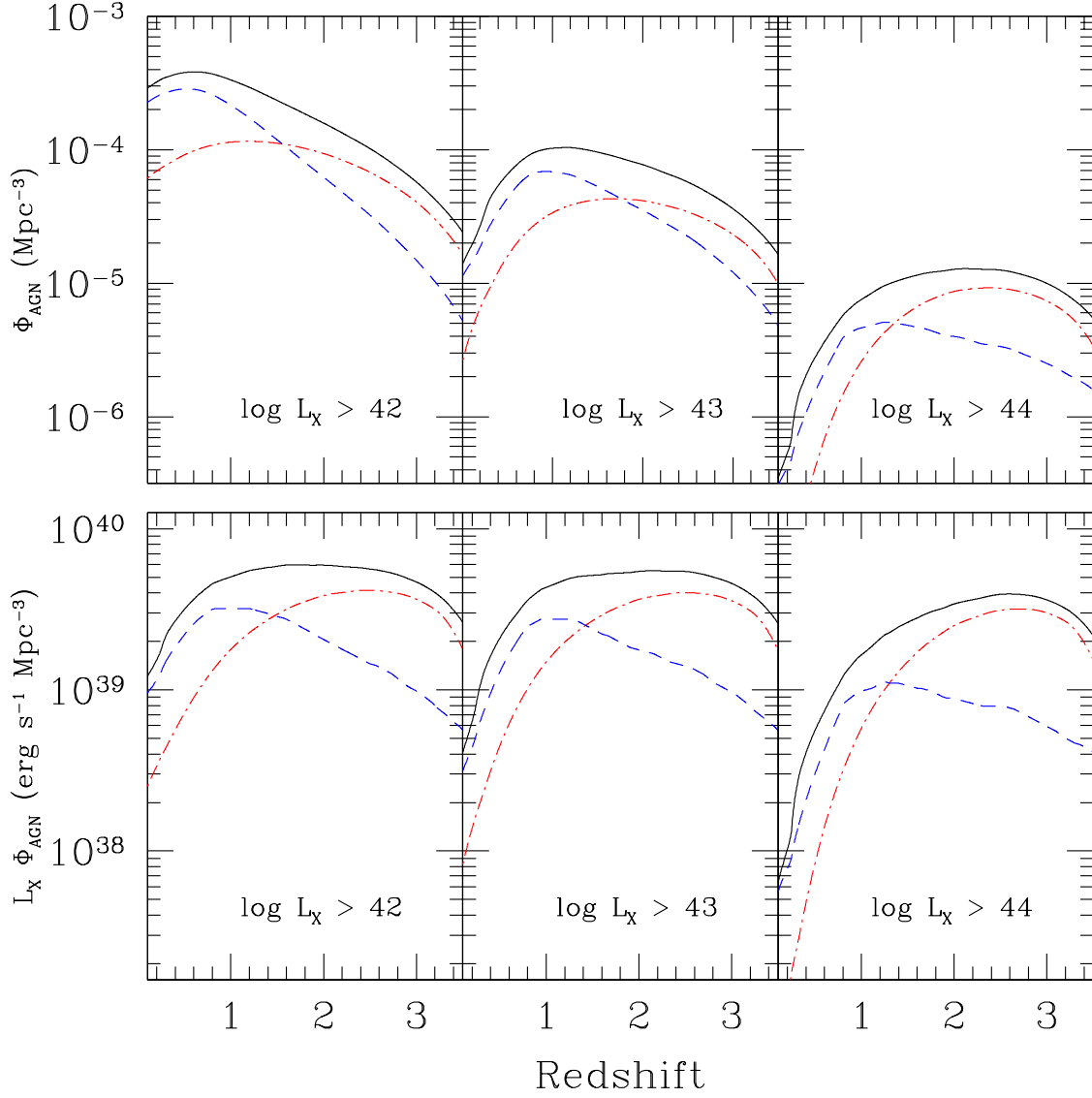
Fig. 7.— The space and luminosity density of AGN as a function of redshift predicted by the mixed ABHMF model. The top row shows the space density of AGN for $\log L_X > 42$, 43, and 44. The bottom row shows the luminosity density of AGN for $\log L_X > 42$, 43, and 44. The line styles are the same as in Figure 2.